Spatial Variability of Liquid Water Path in Marine Low Cloud: The Importance of Mesoscale Cellular Convection

ROBERT WOOD AND DENNIS L. HARTMANN

University of Washington, Seattle, Washington

(Manuscript received 11 October 2004, in final form 22 September 2005)

ABSTRACT

Liquid water path (LWP) mesoscale spatial variability in marine low cloud over the eastern subtropical oceans is examined using two months of daytime retrievals from the Moderate Resolution Imaging Spectroradiometer (MODIS) on the NASA *Terra* satellite. Approximately 20 000 scenes of size 256 km × 256 km are used in the analysis. It is found that cloud fraction is strongly linked with the LWP variability in the cloudy fraction of the scene. It is shown here that in most cases LWP spatial variance is dominated by horizontal scales of 10–50 km, and increases as the variance-containing scale increases, indicating the importance of organized mesoscale cellular convection (MCC). A neural network technique is used to classify MODIS scenes by the spatial variability type (no MCC, closed MCC, open MCC, cellular but disorganized). It is shown how the different types tend to occupy distinct geographical regions and different physical regimes within the subtropics, although the results suggest considerable overlap of the large-scale meteorological conditions associated with each scene type. It is demonstrated that both the frequency of occurrence, and the variance-containing horizontal scale of the MCC increases as the marine boundary layer (MBL) depth increases. However, for the deepest MBLs, the MCC tends to be replaced by clouds containing cells but lacking organization. In regions where MCC is prevalent, a lack of sensitivity of the MCC type (open or closed) to the large-scale meteorology was found, suggesting a mechanism internal to the MBL may be important in determining MCC type. The results indicate that knowledge of the physics of MCC will be required to completely understand and predict low cloud coverage and variability in the subtropics.

1. Introduction

Low clouds over the oceans are spatially variable on scales from meters to hundreds of kilometers (Cahalan and Snider 1989; Davis et al. 1996; Marshak et al. 1997; Wood and Taylor 2001). This spatial cloud variability needs to be understood because of its importance in cloud–radiation interactions (Cahalan et al. 1994; Barker 1996a,b; Oreopoulos and Davies 1998a,b; Rossow et al. 2002), and in controlling the precipitation rate (Rotstayn 2000; Pincus and Klein 2000; Larson et al. 2001b; Wood et al. 2002; Stevens et al. 2005).

Parameterizing low cloud cover and spatial variability in large-scale numerical models continues to be a challenge. There has been considerable recent focus upon designing cloud schemes that predict the cloud fraction (CF) and internal variability using a saturation deficit probability distribution approach (e.g., Smith 1990; Tompkins 2002). Testing these schemes using observational data has lagged behind their conception. These schemes contain implicit relationships between the distribution moments and the cloud cover that are amenable to examination using observations. Key outstanding questions are: What relationships are observed between the CF and internal cloud variability in cloud liquid water path (LWP)? Can these relationships be modeled using simple ideas?

It is common for low clouds, most of which occur within the marine boundary layer (MBL), to self-organize into mesoscale cellular convection (MCC; see reviews by Agee et al. 1973; Atkinson and Zhang 1996), with dominant horizontal scales much greater than the depth of the MBL. Mesoscale cellular convection can exist in the open form (where narrow regions of cloud form around the cell edges with broad regions of clearing between), the closed form (where broad regions of thick stratiform cloud form in the cell centers with relatively narrow regions of thinning or clearing at the

Corresponding author address: Dr. Robert Wood, Atmospheric Sciences, University of Washington, Seattle, WA 98195.
E-mail: robwood@atmos.washington.edu

edges), or as isolated cells with no clear organization. The MCC aspect ratios (cell center separation: MBL depth) reported in field studies are typically 3–40 (Atkinson and Zhang 1996), significantly larger than those (usually 2–4) found in Bénard–Rayleigh convection. MCC is the predominant cloud structure for stratocumulus when the boundary layer is deeper than 1 km (Atkinson and Zhang 1996) and is found less often in very shallow stratus-topped boundary layers. A qualitative climatology of closed and open MCC prevalence over the global oceans was introduced by Agee et al. (1973), showing that closed MCC forms preferentially over cold ocean currents and open MCC forms preferentially over warm ocean currents. Little work has been carried out, however, to quantitatively link cloud cover and spatial variability to the cell types and scales associated with MCC.

In this paper we examine aspects of the mesoscale spatial variability in low clouds over the subtropical eastern oceans, where these clouds are extensive, using satellite data. We use LWP derived from visible retrievals as it is directly related to thermodynamic and structural characteristics. Our chief motivation for this work is a desire to quantify the relationships between important cloud characteristics (CF and moments of the LWP distribution), to examine how these vary with mesoscale cellular convection characteristics, and to better understand their associations with the large-scale meteorology.

Section 2 describes the data and analysis methodology. In section 3, we examine links between CF and the cloud LWP variability. Section 4 explores links between LWP spatial variability and mesoscale cellular convection. In section 5 we investigate meteorological controls on MCC type and scale. Section 6 presents a discussion and suggestions for future work.

2. Data and methodology

a. Satellite data and physical parameter estimation

We use 1 km (at nadir) data from the Moderate Resolution Imaging Spectroradiometer (MODIS) on the National Aeronautics and Space Administration (NASA) *Terra* sun-synchronous satellite (King et al. 1992). The MODIS cloud product uses visible/near-IR radiances (King et al. 2003) to derive optical thickness τ and near-cloud-top effective radius $r_{e,\text{top}}$ resolution for cloudy pixels in daytime (~1030 LST) scenes. Only those pixels within 45° of nadir (i.e., the central 1030 pixels of the scan) are used. The MODIS cloud mask (Ackerman et al. 2002) is used to determine which pixels are cloudy, and therefore the CF. Data from each granule are interpolated onto a 1 km × 1 km across- and along-track grid (1280 km across track, 2030 km along track).

Estimation of LWP from $r_{e,\text{top}}$ and τ requires a model of the cloud vertical structure. Often, the cloud is modeled as having constant liquid water content (LWC) and $r_{e,\text{top}}$ in the vertical (e.g., Han et al. 1994), which gives

$$\text{LWP} = \frac{2}{3}\rho_w \tau r_{e,\text{top}},$$

with ρ_w the density of liquid water. However, observations of boundary layer clouds indicate that the liquid water content is often an approximately linear function of height above cloud base, and that the cloud droplet concentration is approximately constant with height (e.g., Nicholls and Leighton 1986; Brenguier et al. 2000; Wood 2005). This model, used here, results in a relationship

$$\text{LWP} = \frac{5}{9}\rho_w \tau r_{e,\text{top}},$$

giving LWP values a factor of 5/6 = 0.83 times those using the constant LWC, r_e model. The detection limit for LWP is roughly that corresponding to a visible optical thickness of $\tau = 1$, although some lower values are reported for cloud-classified pixels. We modify the cloud mask to classify as clear, pixels with LWP < 5 g m^{-2}. This does not have a marked effect upon the derived statistics, but it is important when comparing with analytical models of the LWP probability density function. Based upon the optical thickness error analysis of Pincus et al. (1995), and the error analysis presented in King et al. (1997), a conservative error for the pixel-level LWP estimates is roughly 20%–40%, although the relative error from pixel to pixel is likely to be considerably less than this.

MBL depth z_i is estimated from the difference between sea surface temperature and cloud-top temperature, using vertical structure from the MBL model of Park et al. (2004), as described in Wood and Bretherton (2004). Estimates of the accuracy of this technique suggest that the uncertainty in each z_i estimate is approximately 200–300 m (Wood and Bretherton 2004).

b. Scene selection

Our basic unit of analysis is a "scene," a 256 × 256 km^2 portion of the MODIS swath. Scenes containing only warm cloud are selected using the MODIS thermal IR cloud-top temperature (Ma et al. 2000). Only wholly oceanic scenes are analyzed. Some scenes are rejected because of clear instrumental or calibration errors resulting in unphysically large τ. The occurrence of such scenes is uncorrelated with cloud characteristics and so

TABLE 1. Details of the regions examined in this study.

Region	Longitude range	Latitude range	Period (mm/dd/yy)	Scenes analyzed (number)
NE Pacific	110°–150°W	10°–50°N	08/20/00–10/31/00	7803
SE Pacific	70°–120°W	30°S–10°N	09/01/00–10/31/00	12 992

should not bias the results. Scenes are oversampled at increments of 128 km in each direction, which gives an approximate restoration of the degrees of freedom lost through data windowing.

Two regions of the east Pacific dominated by low cloud are chosen for this study (see Table 1). All available data from September/October 2000 are used. Figure 1 shows the regions, together with contours that give the fraction of MODIS scenes accepted for analysis. The International Satellite Cloud Climatology Project (ISCCP; Rossow and Schiffer 1991) 16-yr climatological mid- + high cloud amount for September/October (assuming random overlap) is also shown. Over much of the two regions, particularly in the southeast (SE) Pacific, the mid- + high cloud amount is less than 10%–15% and the fraction of scenes analyzed exceeds 50%, demonstrating the dominance of low cloud, and the lack of high clouds to the east of the subtropical gyres. This fraction decreases both equatorward, because of the presence of clouds associated with deep convection, and toward the midlatitudes, where deep frontal clouds are prevalent. The curious peak in ISCCP mid- + high cloud off the coast of southern Peru/northern Chile probably reflects a misdiagnosis of low clouds as midlevel clouds caused by the extremely strong inversions representative of this region.

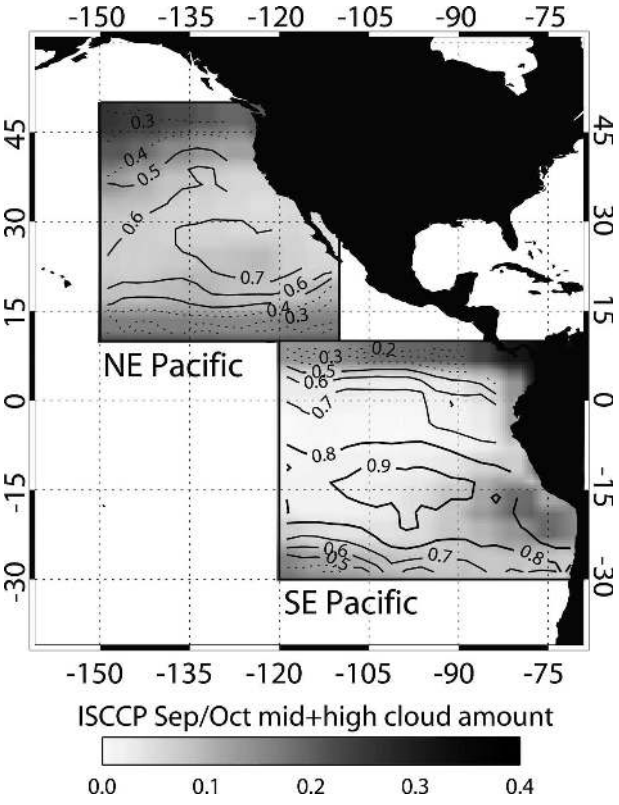

FIG. 1. The two regions (NE and SE Pacific) in this study. Contours show fraction of 256 km × 256 km scenes containing only warm cloud ($T_{top} > 273$ K). Grayscale shading shows ISCCP mid- + high cloud amount for September/October 1984–99.

c. Example scenes

To demonstrate the range of observed cloud variability in the subtropical MBL we use four test scenes containing boundary layer cloud types and structures representative of the range found in MBL clouds (Fig. 2). These will be used to demonstrate the analysis methods described below. Scene a (Fig. 2a) contains relatively homogeneous stratus without clearly defined mesoscale cellular convection, which is common in near-coastal waters in the northeast (NE) Pacific. Scene b (Fig. 2b) contains relatively unbroken stratocumulus cloud with small mesoscale convective cells typical of the extensive stratocumulus sheets over the oceans to the west of continents. Scene c (Fig. 2c) contains large stratocumulus cells with breaks typical of the transition regions in the trade wind boundary layer. Scene d (Fig. 2d) contains open-celled MCC. Dates and locations, together with a number of parameters (that will be explained below) obtained for each of these scenes are given in Table 2.

d. Probability density functions, power spectra, and length scales

This study is concerned with the spatial variability of LWP and its dependence upon spatial scale. We use probability density functions (PDFs), and power spectral analysis to examine variance as a function of spatial scale.

Probability density functions (PDFs) of LWP for the cloudy pixels in each scene are derived. From these PDFs, various moments are estimated and used to examine connections between cloud variability and CF. We denote the mean and standard deviation of LWP

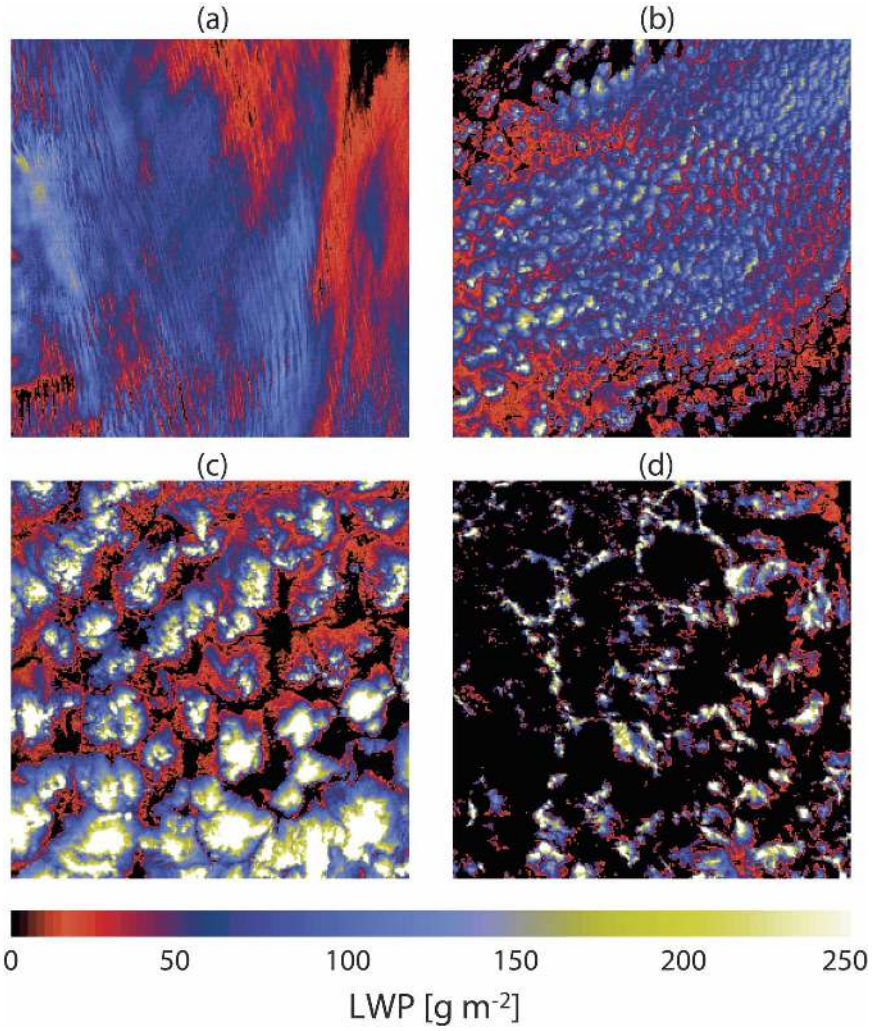

FIG. 2. Example scenes of MODIS LWP in boundary layer cloud showing wide variability in cloud structure. Each scene size is 256 km × 256 km at 1-km resolution. Image times and locations are given in Table 2.

over the cloudy pixels of the scene as $\overline{\mathrm{LWP}}$ and σ_{LWP}, respectively. Following Barker (1996b) and Oreopoulos and Davies (1998a) we use $\gamma_{\mathrm{LWP}} = (\overline{\mathrm{LWP}}/\sigma_{\mathrm{LWP}})^2$ as a nondimensional homogeneity parameter. Figure 3 shows a comparison of the LWP PDFs for the four example scenes. A clear shift from a modal to a nonmodal PDF form is seen with decreasing cloud cover. Accompanying this shift is a general decrease in γ_{LWP}

TABLE 2. Characteristics of the four test images shown in Fig. 2. Parameters listed are cloud fraction CF, characteristic scale of the cells λ_1 and of the cloud structures λ_2, mean liquid water path $\overline{\mathrm{LWP}}$, the ratio of square of the mean to the variance of LWP for cloudy pixels only (γ_{LWP}), liquid water path skewness S_{LWP}, scene type (no MCC, N; closed MCC, C; open MCC, O), and the boundary layer depth z_i.

Image	Date	Location (lat, lon)	CF	λ_1 (km)	λ_2 (km)	$\overline{\mathrm{LWP}}$ (g m^{-2})	γ	S_{LWP}	Type	z_i (m)
(a)	17 Oct 2000	36°N, 125°W	0.99	5.4	N/A*	59	5.02	0.51	N	610
(b)	18 Aug 2000	30°N, 131°W	0.88	10.9	10.3	64	3.13	1.45	C	760
(c)	18 Aug 2000	26°N, 135°W	0.86	38.5	48.2	85	1.35	1.38	C	1100
(d)	13 Oct 2000	11°S, 97°W	0.32	35.7	10.1	92	1.24	1.72	O	1020

* Characteristic scale undetermined.

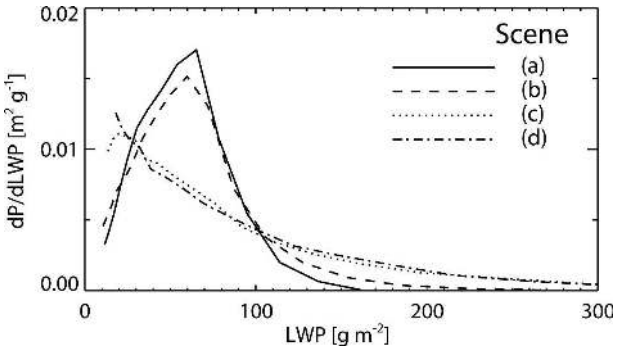

FIG. 3. Examples of LWP PDFs for the four test scenes shown in Fig. 2.

as the cloudy fraction of the scene becomes more inhomogeneous, together with an increase in the skewness of the distribution (Table 2). These links are explored more systematically in section 3.

For each scene we derive the two-dimensional power spectrum as a function of total wavenumber k, where $k^2 = k_x^2 + k_y^2$ and k_x and k_y are the wavenumbers along the axes of the square scene. The image is first detrended by removing the best-fit plane and then windowed using a Welch window. Spectra for the four test scenes are shown in Fig. 4. We find in general that spectra for both open and closed MCC usually exhibit a peak at some length scale (this length scale we call λ_1). Power-law scaling is generally found at large k. The scale at which the spectrum diverges from the power law we label as λ_2. Closed MCC spectra diverge from the power law at a scale close to the peak scale (i.e., $\lambda_1 \approx \lambda_2$, as in Figs. 4b,c), but for open MCC the divergence from power-law behavior occurs at a scale somewhat smaller than the cell scale (i.e., $\lambda_1 > \lambda_2$, as in Figs. 4b,c). Visual inspection of many scenes leads to the conclusion that λ_1 and λ_2 can be interpreted as the approximate cell diameter and typical cloud size, respectively. For closed cells these are approximately the same because the gaps between clouds are quite small. Open MCC tends to consist of small clouds that form around the perimeter of a larger cellular structure and so λ_2 is often considerably smaller than λ_1.

Automatic methods are used to determine the length scales λ_1 and λ_2 from the power spectral data. Tests using synthetic fractal scenes with spatial variability characteristics representative of low clouds reveal rms errors in the estimated values of λ_1 of 10%–20%, with a tendency for systematic underestimation that increases from approximately 3 km for $\lambda_1 = 20$ km to 6 km for $\lambda_1 = 50$ km. In some cases the power-law behavior is either not present or limited to scales similar to the Nyquist frequency (0.5 km^{-1}). In these cases λ_2 is undefined. Similarly, some of the scenes do not contain a peak in the power spectrum other than that introduced artificially by data windowing. In such cases λ_1 is undefined. Table 2 shows values of λ_1 and λ_2 for the example scenes. Note that it is possible that scenes without clearly defined mesoscale cellular convection, such as scene a in Fig. 2, can have λ_1 defined. In these cases, roll-like structures give rise to the power spectral peak. Power spectra and their relationship with LWP variance are further explored in section 4.

e. Neural network scene type classification

The LWP PDF and the power spectrum are used together to classify scenes into four categories that encompass the range of mesoscale (1–100 km) structures in low clouds: (i) clouds with no clear identifiable cellularity, (ii) closed MCC, (iii) open MCC, and (iv) clouds containing cells but with no clear organization. We use a three-layer back propagation neural network (Castleman 1996; Atkinson and Tatnall 1997; Clark and Boyce 1999; Schroder et al. 2002), with a feature vector combining 32 elements describing the LWP power spectrum and 40 elements characterizing the LWP PDF. Approximately 1000 scenes were classified by eye as belonging to one of the categories (i)–(iv) above, and this ensemble was randomly split into two to provide training and verification datasets. Training is carried out until the misclassification in the verification dataset ceases to decrease. We obtained an 85%–90% classification accuracy for the trained network. Visual inspection shows the misclassified scenes tend to have features common to two categories, that is, those more difficult to classify for the human observer. The neural network weights derived from the training process are then applied to all MODIS data from the NE and SE Pacific to provide a scene-by-scene classification. Figure 5 shows a selection of 16 MODIS scenes, arranged by scene type, that have been successfully classified using the neural network algorithm.

f. Reanalysis data

Reanalysis data from the National Centers for Environmental Prediction–National Center for Atmospheric Research (NCEP–NCAR) reanalysis (Kistler et al. 2001) are used to investigate links between large-scale meteorology and mesoscale spatial variability. Our methodology is to obtain a set of pertinent reanalysis variables for each of the MODIS scenes analyzed. Reanalysis data are available 4 times daily on a 2.5° × 2.5° grid, and include sea surface temperature data

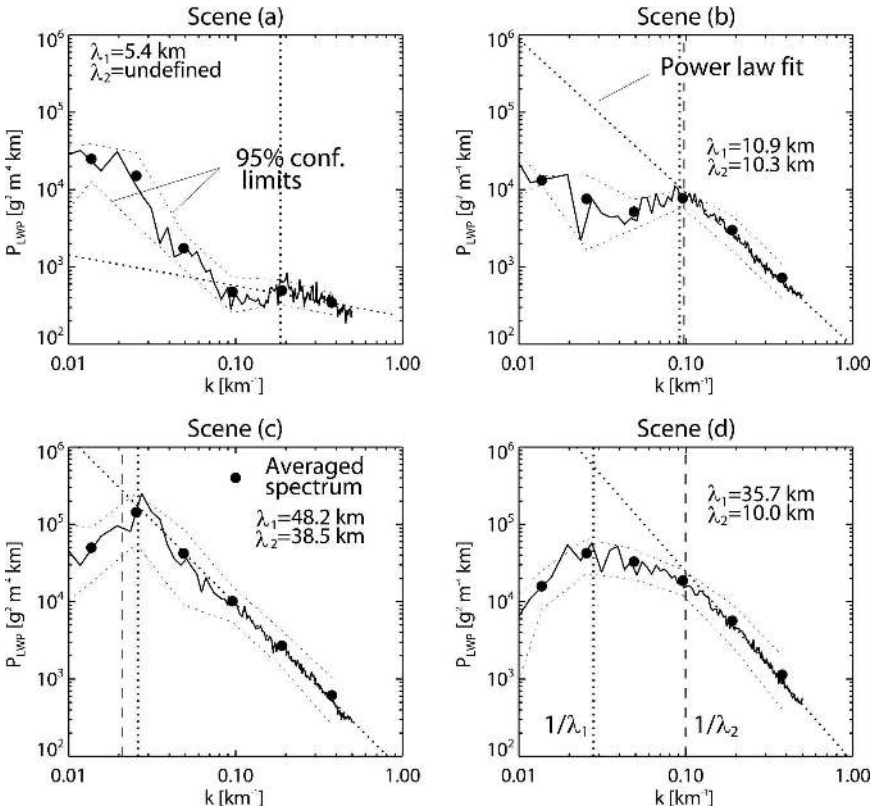

FIG. 4. Power spectra calculated using a 2D FFT for the four example scenes shown in Fig. 2. The unsmoothed spectra are shown using the solid line. Spectra are normalized so that $\int_0^\infty P_{\mathrm{LWP}} dk = \sigma^2_{\mathrm{LWP,\ all}}$ where $\sigma_{\mathrm{LWP,\ all}}$ is the standard deviation of LWP (including cloud-free regions where LWP = 0). Averaged spectra are shown using filled circles and approximate 95% confidence limits are given by the light dotted line. The filled triangle on the wavenumber axis shows the mean wavenumber used to determine the power-law fit to the large k end of the observed spectra (thick dotted line). The two characteristic length scales are defined as λ_1, the wavelength of the highest wavenumber peak in the averaged power spectrum; λ_2, the minimum wavenumber at which the 95% confidence limit of the spectrum exceeds the fitted power law. These scales correspond approximately to cellular diameters and cloud sizes, respectively.

(Reynolds and Smith 1994). Trilinear interpolation is used to determine the values of the reanalysis variables at the MODIS scene-center locations and times. We consider three large-scale variables derived from reanalysis in this study: lower-tropospheric stability (LTS $= \theta_{700} - \theta_0$, where θ_{700} and θ_0 are the potential temperatures at 700 hPa and the surface, respectively); large-scale vertical motion at 850 hPa (w_{850}); and sea surface temperature advection $\mathbf{U} \cdot \nabla \mathrm{SST}$, where $\mathbf{U}$ is the surface wind and SST is the sea surface temperature. Because it is known that there exists a sizeable diurnal cycle in surface divergence and subsidence rates above the MBL (Dai and Deser 1999), we use the mean w_{850} for the 24-h period centered on the time of the MODIS overpass. This is unnecessary for the other reanalysis parameters as their diurnal cycles are much weaker.

3. CF and LWP variability

The early work of Barker (1996b) presented the first observational evidence that cloud internal variability and CF might be linked, with homogeneous clouds also being those with the most extensive cloud cover. However, the limited sample of high-resolution satellite images in the Barker study was insufficient to fully explore the relationship between cloud homogeneity and CF. Similar findings were reported by Pincus et al. (1999) using simultaneous observations from ships and satellite, but no explicit classification by CF was carried out. The general issue here is to what degree can associations between cloud cover and the internal variability of the cloud be represented using simple ideas. From a conceptual viewpoint, it is relatively straightforward

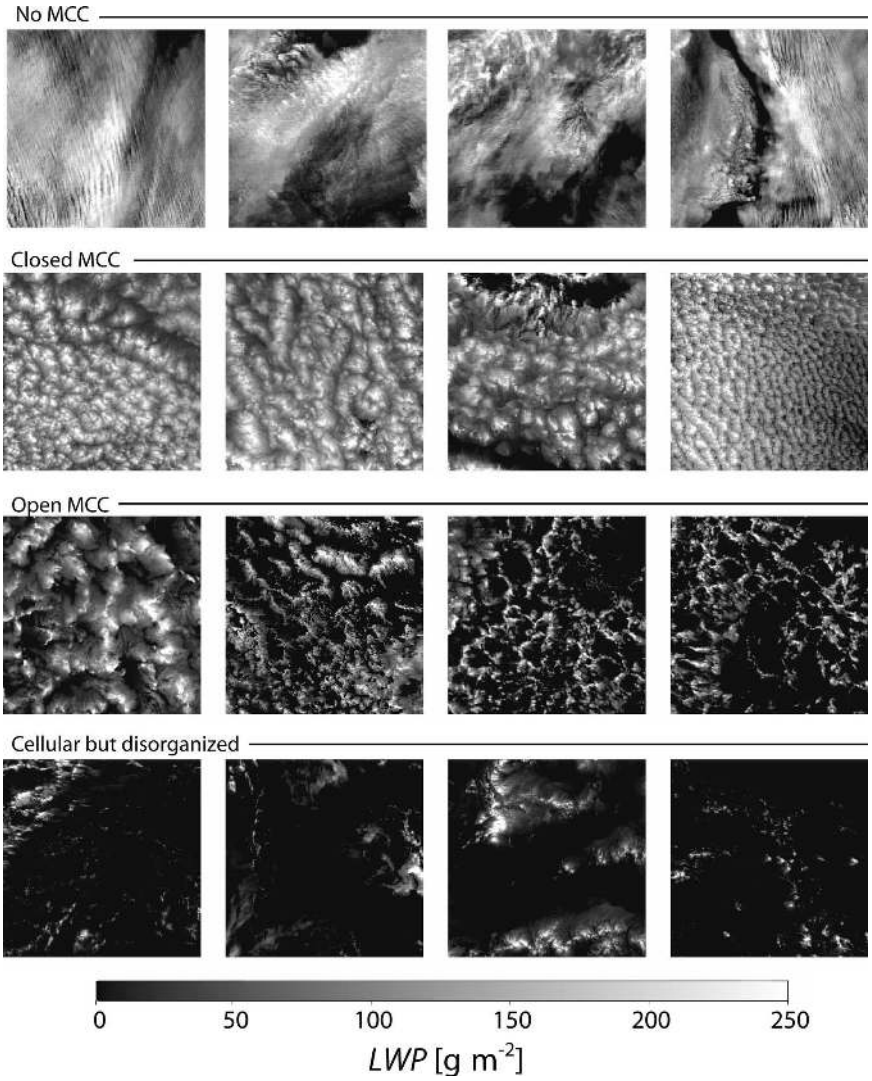

FIG. 5. Selection of MODIS scenes categorized by the neural network scene classification type.

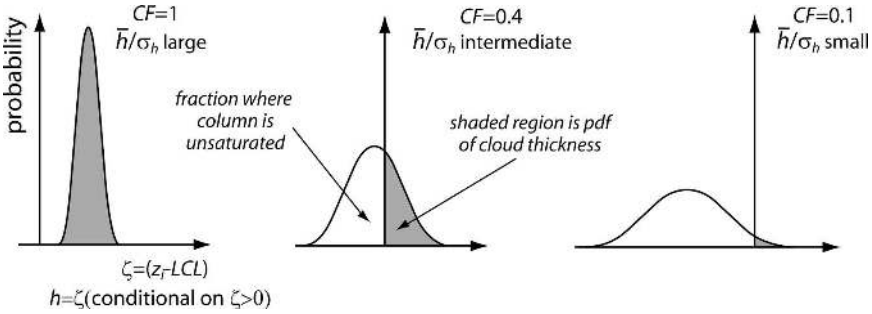

FIG. 6. Links between nondimensional cloud heterogeneity and CF for a simple PDF model of cloud thickness variability. The horizontal axis represents the difference in height h between the inversion base height z_i and the LCL, so that the shaded areas represent cloudy regions and the unshaded regions are regions without cloud.

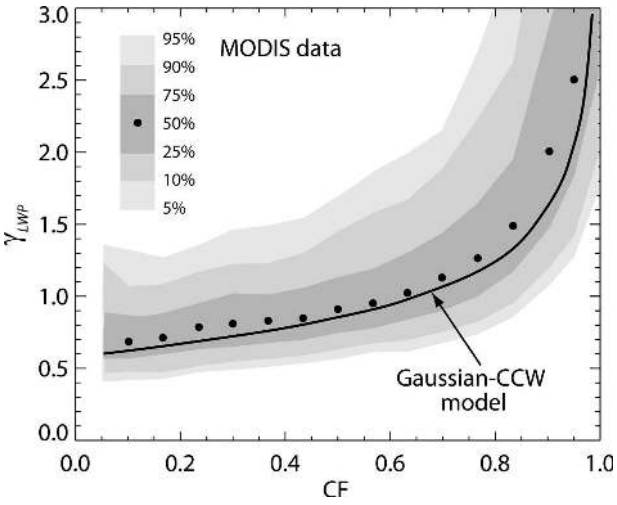

FIG. 7. The CF-conditional probability contours (shaded) of γ_{LWP} for the SE Pacific MODIS scenes. The contours represent 5th, 10th, 25th, 75th, 90th, and 95th percentiles. Median CF-conditional values of γ_{LWP} are also shown (filled circles) together with the median values for the Gaussian–C97 model. Note that the unique nature of the CF–γ_{LWP} relationship in the Gaussian–C97 model is violated when a minimum LWP threshold is applied, as must be done to properly compare with the MODIS data. This results in some spread in the model CF–γ_{LWP} relationship, but that spread is minimal compared with the spread in the MODIS data themselves.

to argue for such a connection using the simple boundary layer cloud model of Considine et al. (1997, hereafter C97), which builds upon ideas from statistical cloud schemes (Sommeria and Deardorff 1977; Mellor 1977) originally intended to parameterize small-scale variability in the marine boundary layer. In the C97 model the cloud-top height is assumed constant and equal to the height of the base of the inversion layer (the MBL depth z_i) , and the lifting condensation level (LCL) is assumed to be a random variable with a particular PDF form. The parameter $\zeta = z_i - \text{LCL}$ is equal to the cloud thickness h for columns where $\zeta > 0$. Where $\zeta \leq 0$, the MBL column is cloud free. Figure 6 demonstrates graphically that for a given PDF form (in this case Gaussian) this model yields a relationship between cloud thickness homogeneity for the cloudy columns and CF, with increased heterogeneity (decreased $\overline{h}/\sigma_h$, where $\overline{h}$ and σ_h are the mean and standard deviation of h, respectively) associated with lower cloud cover.

Assuming an adiabatic cloud layer, so that LWP and h are related, the C97 model can be expanded to yield the PDF of LWP (Considine et al. 1997; Wood and Taylor 2001). It has been found that a Gaussian PDF form is broadly consistent with observations of both total water content (Wood and Field 2000; Larson et al. 2001a) and cloud thickness (Wood and Taylor 2001) variability in overcast MBL clouds, but much less is known about these links at smaller CFs. It can be shown (e.g., Wood et al. 2002; Jeffery and Austin 2003) that for a Gaussian PDF form, the C97 model yields a unique relationship between the CF and γ_{LWP}.

Predictions of the Gaussian–C97 model are tested against all the SE Pacific satellite data in Fig. 7. An almost identical relationship is found for the NE Pacific data (not shown). The general trend of increasing homogeneity with increasing CF is borne out in the data, and the median CF-conditional values of γ_{LWP} are very close to the median value for the Gaussian–C97 model. There does appear to be a slight tendency for the observed values of γ_{LWP} to be greater than those from the model that tests suggest could reflect statistical inhomogeneity within MODIS scenes. As an additional

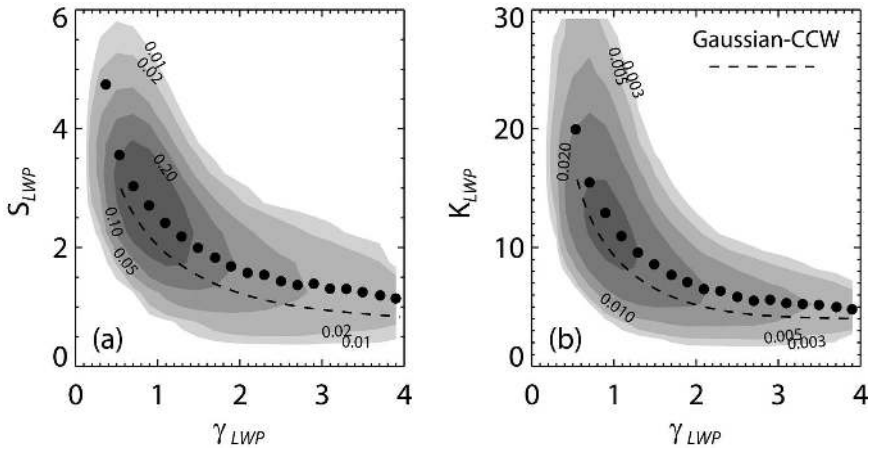

FIG. 8. (a) Skewness–γ_{LWP} and (b) kurtosis–γ_{LWP} frequency distribution (contours) from all SE Pacific MODIS scenes. Median γ_{LWP}–conditional values of skewness S_{LWP} and kurtosis K_{LWP} are shown from the data (filled circles) and for the Gaussian–C97 model with a LWP threshold of 5 g m^{-2}.

demonstration of links between LWP PDF parameters, we examine the relationship between the homogeneity parameter γ_{LWP} and higher moments of the LWP distribution; that is, the skewness and kurtosis (Fig. 8). The observations show decreasing skewness and kurtosis as γ_{LWP} increases. This is consistent with the example PDFs shown in Fig. 3, with a trend toward more skewed, less bell-shaped structures as the CF and homogeneity decrease together. Again, the Gaussian–C97 model represents this general trend in the behavior of the higher moments quite faithfully, indicating its utility as a simple description of the links between cloud cover and LWP variability in marine low cloud. In the following section we explore the relationships between the cloud variability and characteristics of the mesoscale cellular convection.

4. Cloud variability and mesoscale cellular convection

In the previous section evidence was presented demonstrating links between the CF and the cloud LWP PDF. Insight into the role that different convective organization plays in determining the PDF characteristics over the subtropical eastern oceans is provided in Fig. 9, which shows the distribution of cloud mean LWP, CF, and γ_{LWP} for the four categories of scene type discussed in section 2e. Much higher CF and more spatial homogeneity (higher γ_{LWP}) is found for closed MCC compared with open MCC. The no-MCC scenes have a broad distribution of CF and tend to have low mean LWP. These scenes are often found where stratus/stratocumulus sheets are in their early stages of formation.

It is noteworthy that for scenes with CF > 0.3, roughly 60% of all scenes are classified as either open or closed MCC, and for CF > 0.6, this rises to 75%. This highlights that mesoscale cellular convection is the predominant form for the organization of MBL clouds over the cloudy regions of the eastern subtropical oceans.

We next examine the scale-dependent properties of the cloud fields using spectral analysis. The horizontal scale of the MCC, as defined by λ_1 (section 2d above) is used as a basis for compositing LWP power spectra (Fig. 10). An approximate power-law scaling of the high wavenumber tail $k > \lambda_1^{-1}$ with an exponent in the range 1.4–2.0 is found in accordance with previous observations (e.g., Cahalan and Snider 1989; Wood and Taylor 2001). It is also clear that increasing MCC cell size is associated with an increase in variance and that most of the additional variance as λ_1 increases is coming from scales close to the cell scale. This is strong evidence that mesoscale cells are dominating the sub-256-km spatial variability in marine low clouds. This is further confirmed in Fig. 11, which shows a tendency for decreasing homogeneity with increasing cell scale λ_1 for both open and closed MCC. However, although the cell scale appears to be an important factor affecting the cloud structure, it is clear from the fairly broad range of γ_{LWP} at any particular value of λ_1 that variability of the LWP PDF characteristics is not entirely explained by the size of the cells as open and closed scenes have distinct relationships between $\overline{LWP}$, CF, γ_{LWP}, and λ_1. For a particular cell scale, open MCC clouds are considerably more heterogeneous, have lower CF, and slightly lower cloud mean LWP.

5. Associations between environmental state, MCC, and cloud variability

We have seen that the presence or absence of MCC, and the scale of the cells that form when it is present are associated with systematic differences in cloud spatial variability and cover in the subtropical MBL. It is therefore important to examine the environmental states that are associated with the MCC as part of an effort to better understand and parameterize cloud physical properties.

Previous work has shown that low cloud cover in the subtropical MBL is well correlated with lower-tropospheric stability (Slingo 1980; Klein and Hartmann 1993; Klein 1997), and in some regions temperature advection (Klein 1997). In addition, the tropospheric subsidence rate (Wyant et al. 2006) has been shown to be a useful classifier of low cloud cover. MBL depth is also expected to be a key property that can potentially impact the energetics and structural properties of low clouds. Little has been reported, however, about the associations between these variables and mesoscale cellular convection and cloud spatial variability.

In this section we examine whether the magnitude and type of mesoscale spatial variability in low clouds is associated with corresponding changes in large-scale meteorological factors pertinent to the MBL.

a. Geographical variability

Figure 12 shows median values of the scene mean LWP, CF, and γ_{LWP} for $2.5° \times 2.5°$ boxes from the entire dataset. Figure 13 shows the median cell size λ_1. The relative frequency of occurrence of the different scene types is shown in Fig. 14, and the mean z_i and reanalysis surface winds are shown in Fig. 15.

The increase in γ_{LWP} with increasing CF explored in section 3 is clearly seen at the regional level (Fig. 12). There is also the tendency for clouds without MCC near the coasts to have lower mean LWP, although there is no clear relationship further from shore. In general, both the NE and SE Pacific regions show simi-

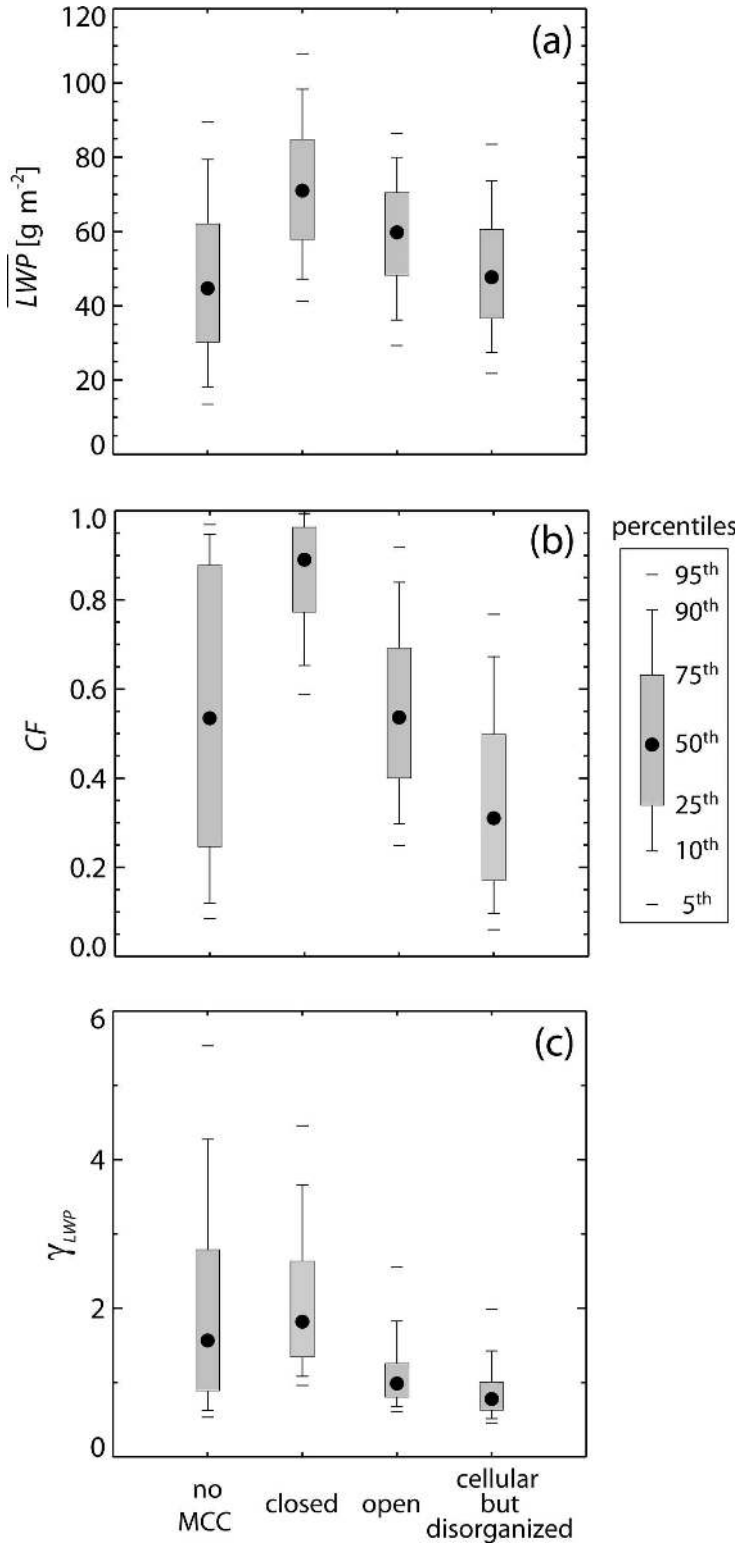

FIG. 9. Probability distributions expressed using box-whisker plots (showing percentiles 5, 10, 25, 50, 75, 90, and 95) of (a) $\overline{\text{LWP}}$, (b) CF, (c) γ_{LWP}, for the four scene types.

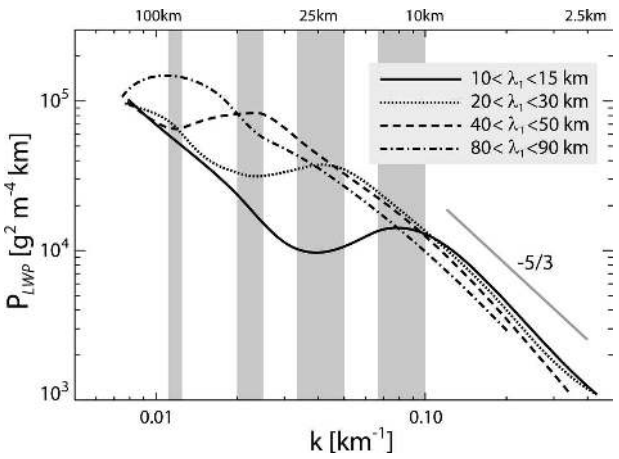

FIG. 10. Averaged power spectra four different ranges of the characteristic cell length scale λ_1. Vertical gray bars indicate extent of λ_1 ranges used for compositing. Data are taken from the NE Pacific region only; composite spectra are almost identical for the SE Pacific data.

lar transitions in the spatial variability characteristics of clouds along climatological trajectories. From the near-coastal regions off California and northern Chile, which feature shallow MBLs with extensive homogeneous clouds (Fig. 12), MBLs tend to deepen downstream (Fig. 15), and we observe an increase in the prevalence of closed MCC (Fig. 14) with an increasing cell size (Fig. 13) and increased heterogeneity. Further downstream, open MCC tends to become more prevalent in both regions, although it is more common in the SE Pacific during this season. Over the warmer waters typical of the eastern ocean trades, cellular but disorganized clouds, with low cloud cover and heterogeneous LWP, are most prevalent. Many of these scenes contain trade wind cumulus clouds, but extensive patches of stratiform cloud within these scenes constitute most of the cloud cover. We further explore the links with MBL depth and large-scale meteorology in the following sections.

b. MBL depth

The frequency of different scene types classified by MBL depth (Fig. 16) confirms the prevalence of clouds without MCC being prevalent in the shallowest MBLs, where MCC is uncommon. The relative frequency of closed MCC peaks at $z_i \approx 900$ m and then decreases for deeper MBLs. Open MCC is most commonly observed

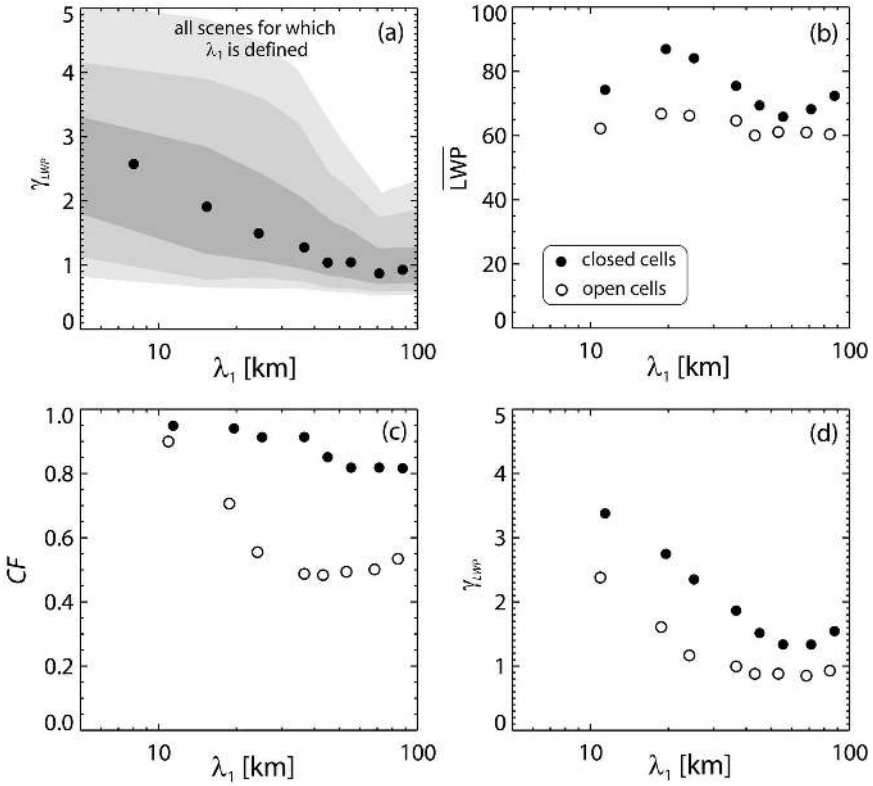

FIG. 11. (a) Normalized homogeneity parameter γ_{LWP} probability density function conditional on cell size for all MODIS scenes where λ_1 is defined with shading the same as for Fig. 7. Median value of (b) λ_1-conditional cloud $\overline{LWP}$, (c) CF, and (d) γ_{LWP} for scenes classified as closed and open mesoscale cellular convection.

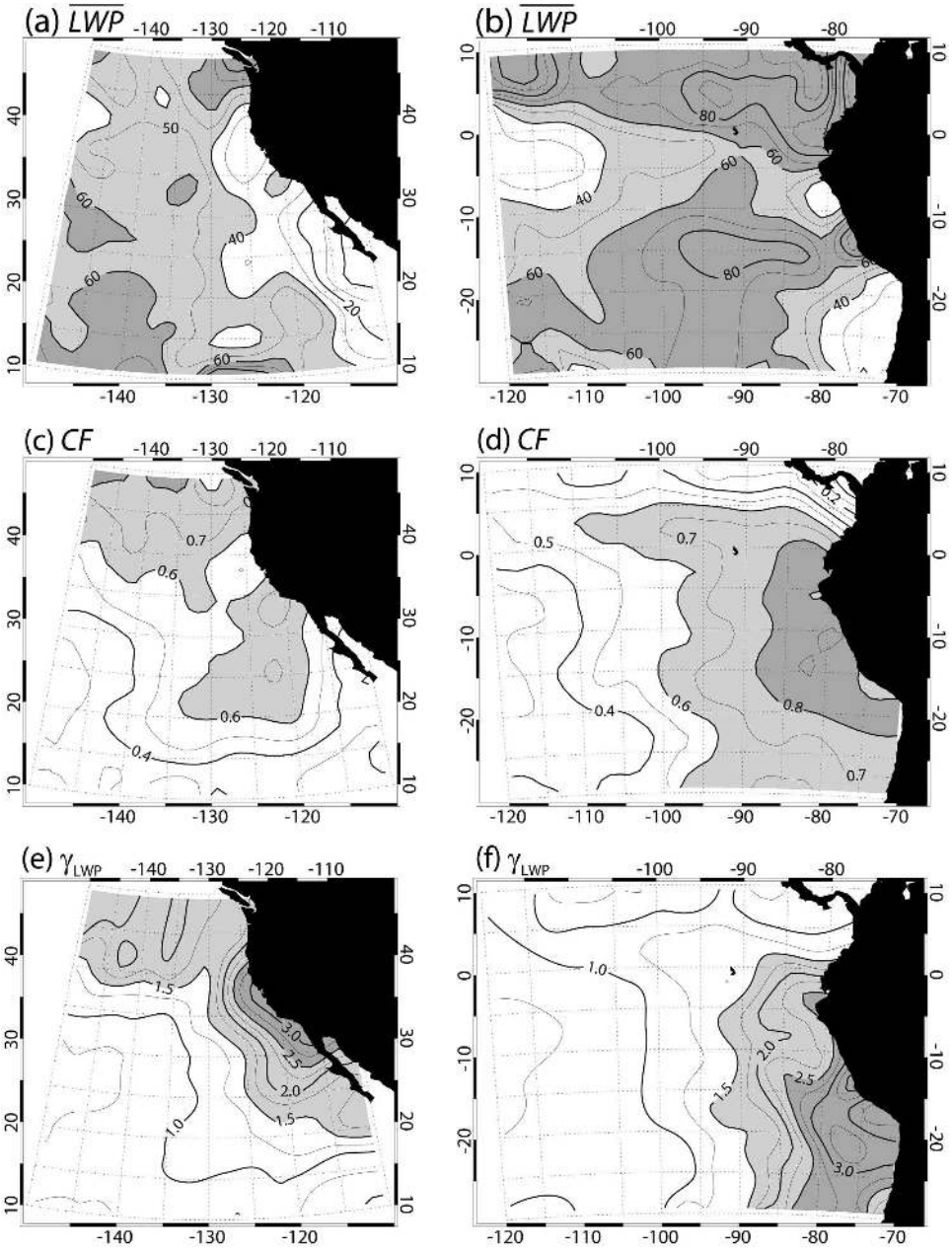

FIG. 12. Climatological mean value of (a), (b) $\overline{\text{LWP}}$, (c), (d) CF, and (e), (f) climatological median value of γ_{LWP} for all September/October MODIS scenes in the NE and SE Pacific.

in MBLs in the $1000 < z_i < 1500$ m range, with cellular but disorganized scenes dominating over clearly defined MCC for $z_i > 1500$ m.

In the previous section we saw how the cloud heterogeneity increased with the cell length scale. Figure 17 shows the relationship between cell size and MBL depth for open and closed MCC. For $z_i < 800$ m open MCC rarely occurs, and MCC of either kind is much less common than noncellular clouds. As the MBL deepens, MCC becomes the dominant form and λ_1 increases to around 30–40 km for $z_i = 1000$ m. Interestingly, the MCC aspect ratio (λ_1:z_i) is typically in the range from 30:1 to 40:1 and is quite insensitive to whether the MCC type is open or closed. This result carries consequences for theories describing MCC formation mechanisms, especially those that implicate cloud-top radiative cooling as a necessary forcing (e.g., Shao and Randall 1996). At cell sizes of around 50 km, the error analysis (section 2d) indicates that the estimates of λ_1 are biased low by roughly 6 km. If this is

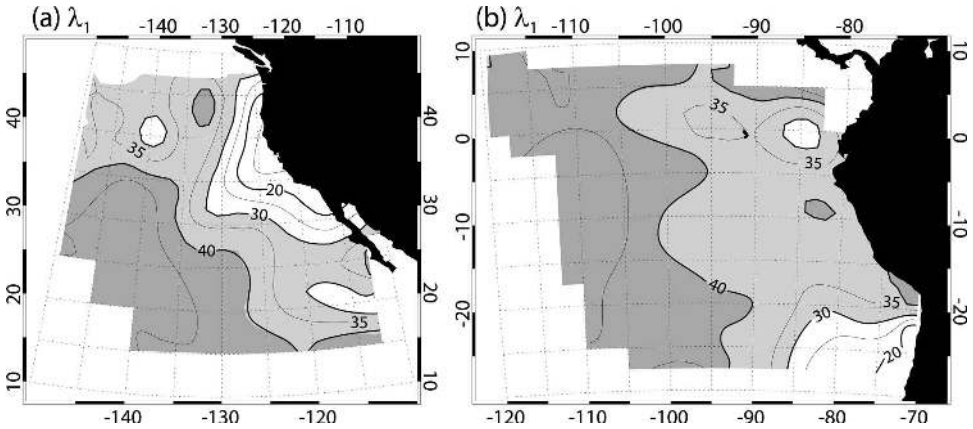

FIG. 13. Median values of the characteristic length scale for all scenes containing MCC (open or closed) with CF > 0.2 for the (a) NE and (b) SE Pacific regions.

taken into account, the results would indicate a more constant aspect ratio in the range 35:1–40:1.

Although there is a tendency for open MCC to become more prevalent than closed MCC as the MBL deepens, we perform an additional analysis for a more controlled study whereby we consider 2.5° × 2.5° boxes where closed and open MCC in total account for over 50% of all scenes (henceforth termed MCC-prevalent boxes). For each of these boxes, we estimate the mean MBL depth (or other large-scale meteorological variables) for open and closed MCC separately and then aggregate these means to estimate a grand mean difference in MBL depth. This analysis reveals that in MCC-prevalent regions, the MBL is actually slightly shallower when open MCC is present than when closed MCC is present. However, the difference is comparable to the sampling error, which suggests the MBL depth is not a key factor controlling the dominant type of MCC that forms in any particular region.

c. Large-scale meteorology

Lower-tropospheric stability (LTS) was found to be strongly correlated with cloud cover in the subtropics at the basinwide spatial scale and on seasonal time scales by Klein and Hartmann (1993). We find a similarly high correlation (Fig. 18) between mean CF and mean LTS for the 2.5° × 2.5° boxes ($r = 0.86$ and 0.90 for the NE and SE Pacific regions, respectively). We find that the mean cloud cover increases by approximately 0.07 for each degree of LTS, which is approximately 20% larger than the value found by Klein and Hartmann (1993).

Given that closed MCC tends to have a considerably higher CF than open MCC, as discussed in section 4, one might assume that at MCC-prevalent locations greater LTS would tend to be associated with closed, as opposed to open MCC. We do find slightly lower LTS, by on average 0.4 K, for open MCC compared with closed MCC in any particular region, but the LTS differences are generally insufficient to explain the much lower CF, by on average 0.3, for open MCC. We also find negligible systematic differences in temperature advection and 850-hPa vertical velocity for open and closed cells for MCC-prevalent regions. We tested the sensitivity to the choice of reanalysis dataset by comparing results with those from the European Centre for Medium-Range Weather Forecasting 40-yr reanalysis and found only small quantitative differences. The apparent lack of dependence of the MCC type upon the large-scale meteorology (and MBL depth) could be caused by unreliable reanalysis data, but this is unlikely because we find good correlations (up to $r = 0.6$) between lower-tropospheric stability and MODIS CF on synoptic time scales (2–30 days) in accordance with Klein (1997; not shown), which suggests that the reanalysis data are reasonably accurate at capturing the synoptic-scale variability over the subtropical eastern oceans. Physical reasons for the insensitivity of MCC type to large-scale meteorology and MBL depth are discussed below.

6. Discussion and conclusions

In this study we have examined characteristics of the spatial variability of cloud LWP in low clouds over the eastern subtropical oceans. Our analysis focuses upon the statistics of approximately twenty thousand 256 × 256 km MODIS scenes containing exclusively low cloud. We identified connections between the CF and the PDF of LWP, including the tendency for heterogeneity to increase as CF decreases, and found that the

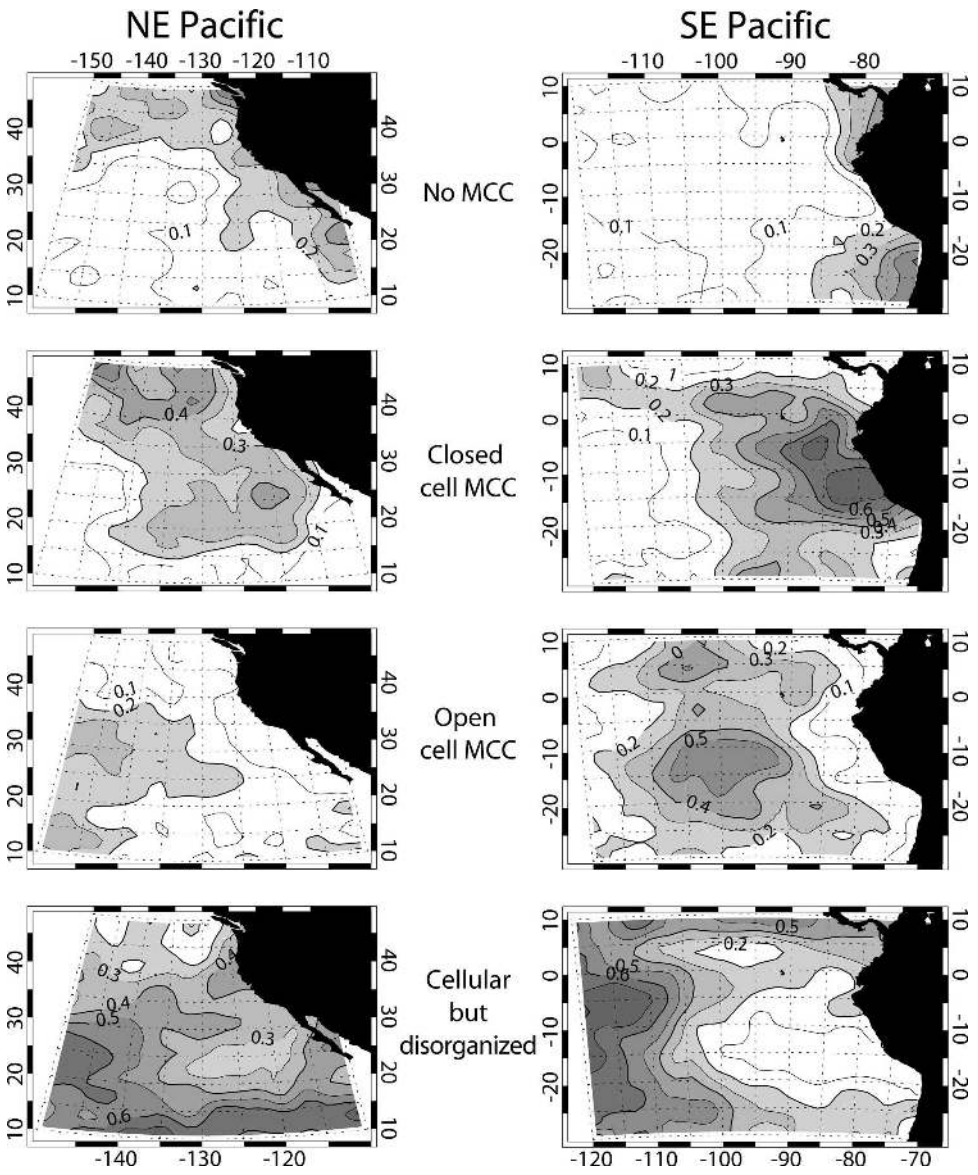

FIG. 14. Frequency of occurrence of no MCC, closed MCC, open MCC, and cellular but disorganized scene types for the NE and SE Pacific.

observed behavior is broadly consistent with a Gaussian model of cloud thickness. If this idea were applied to each grid cell of a global model, the PDF could be used to predict the average radiation and precipitation fluxes (Cahalan et al. 1994; Larson et al. 2001b) within the cell.

We have classified the scenes according to their structural properties and the PDF of LWP. Four categories emerged: unstructured clouds, closed MCC, open-celled MCC, and cellular but disorganized convection. The results indicate that MCC is extremely common over the eastern subtropical oceans, and that scenes without MCC are quite rare and generally limited to near-coastal regions where the MBL is shallow. The findings provide a quantitative corroboration of the climatology of open and closed cellular convection suggested by Agee et al. (1973). Importantly, CF and spatial variability are linked to the presence or absence of mesoscale cellular convection, and its spatial scale. However, further studies are required to determine if MCC is the key driver.

In looking for factors that influence scene variability, we find that the horizontal cell size of the MCC scales well with MBL depth, with aspect ratios typically in the 30:1 to 40:1 range. This scaling, together with the finding that cloud homogeneity and CF also depend upon

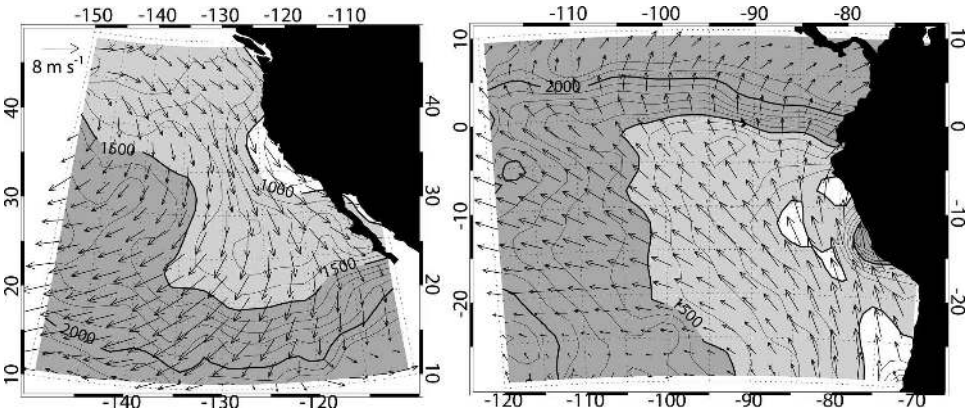

FIG. 15. Mean MBL depth (contours) and NCEP–NCAR reanalysis surface winds (arrows) for all warm cloud scenes in the (a) NE and (b) SE Pacific, September/October 2000.

the MCC scale, suggests an important role for MBL depth in the physical processes that control the cloud radiative properties. This is corroborated in Fig. 18, which shows that the 2.5° × 2.5° mean CF is as well correlated with the mean MBL depth as it is with the mean lower-tropospheric stability.

Our results indicate that lower-tropospheric stability, temperature advection, and 850-hPa vertical velocity do not play a major role in determining the type of MCC, which suggests that instability processes within the boundary layer may be the determining factor. The locations where closed and open MCC are most prevalent (Fig. 14), and qualitative examination of geostationary satellite imagery, suggest that a MCC usually transitions from closed to open. This change often takes the form of small pockets of open cells forming over a few hours within regions of extensive closed cells that then grow to become extensive areas of open MCC. Observations (Stevens et al. 2005; Comstock et al. 2005; Sharon et al. 2006; Petters et al. 2006) suggest that the transition may be driven by feedbacks involving microphysics and precipitation.

The results presented here demonstrate potential new ways satellite and reanalysis data can be combined to examine the spatial variability of low clouds and the large-scale meteorological factors that influence it. Further work could include the extension of this dataset to longer time scales to elucidate the physical mechanisms

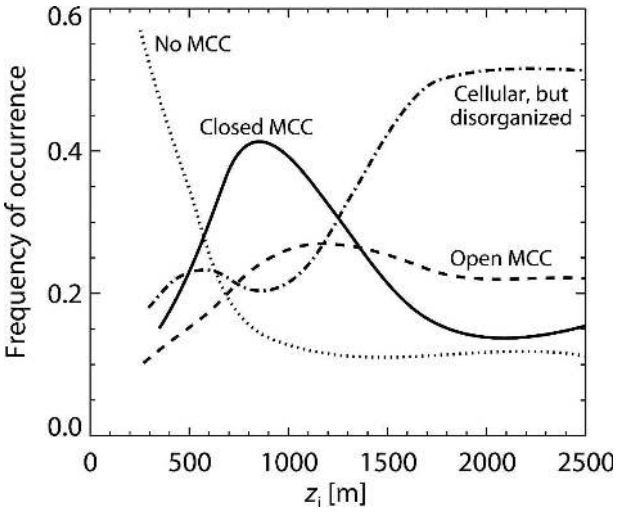

FIG. 16. Frequency of occurrence of the four scene type categories classified by z_i.

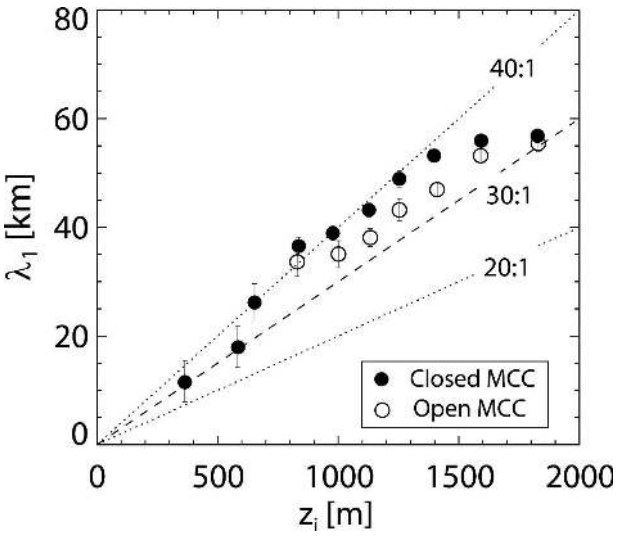

FIG. 17. Median characteristic cell length scale λ_1 binned by z_i for all MODIS scenes (solid circles) over the NE and SE Pacific. The dotted lines denote aspect ratios of 20:1, 30:1, and 40:1. Error bars indicate the approximate sampling error in the median. The solid line indicates the fit described in the text.

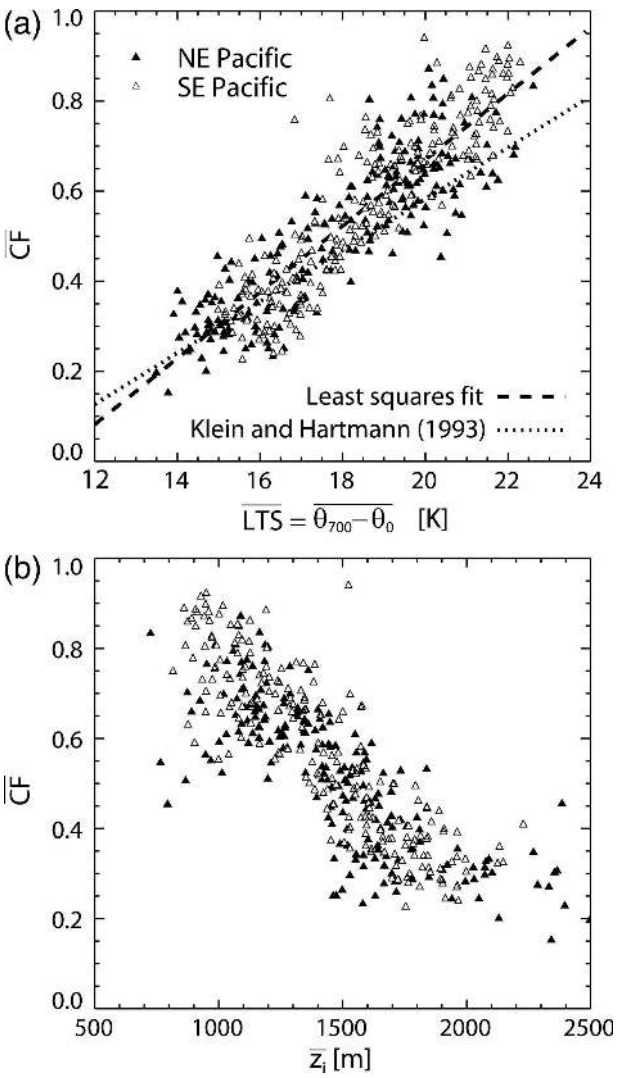

FIG. 18. (a) Two-monthly mean values of MODIS scene CF for each 2.5° × 2.5° region, plotted against (a) mean lower tropospheric stability and (b) mean MBL depth. Data from the SE Pacific region are from south of the equator only where surface sensible heat fluxes do not dominate the MBL energetics. The dotted line in (a) shows the results of Klein and Hartmann (1993) and the dashed line shows the best fit to the MODIS data for the NE and SE Pacific combined.

responsible for the organization of MCC, CF, and variability in the MBL on seasonal time scales.

Acknowledgments. The author thanks the reviewers for their constructive and insightful comments that helped improve the quality of this paper. The work has benefited through fruitful discussions with Philip Austin and Christopher Bretherton. Funding for this work was provided by the NASA EOS Grant NAGS5-10624 (Climate Processes over the Oceans).

REFERENCES

Ackerman, S. A., and Coauthors, 2002, Discriminating clear-sky from cloud with MODIS. MODIS Algorithm Theoretical Basis Doc. MOD35 ATBD-MOD-06, NASA, 115 pp.

Agee, E. M., T. S. Chen, and K. E. Dowell, 1973: A review of mesoscale cellular convection. *Bull. Amer. Meteor. Soc.,* **54,** 1004–1012.

Atkinson, B. W., and J. W. Zhang, 1996: Mesoscale shallow convection in the atmosphere. *Rev. Geophys.,* **34,** 403–431.

Atkinson, P. M., and A. R. L. Tatnall, 1997: Neural networks in remote sensing. *Int. J. Remote Sens.,* **18,** 699–709.

Barker, H. W., 1996a: A parameterization for computing grid-averaged solar fluxes for inhomogeneous marine boundary layer clouds. Part I: Methodology and homogeneous biases. *J. Atmos. Sci.,* **53,** 2289–2303.

——, 1996b: A parameterization for computing grid-averaged solar fluxes for inhomogeneous marine boundary layer clouds. Part II: Validation using satellite data. *J. Atmos. Sci.,* **53,** 2304–2316.

Brenguier, J. L., and Coauthors, 2000: An overview of the ACE-2 cloudy column closure experiment. *Tellus,* **52B,** 815–827.

Cahalan, R. F., and J. B. Snider, 1989: Marine stratocumulus structure. *Remote Sens. Environ.,* **28,** 95–107.

——, W. Ridgway, W. J. Wiscombe, T. L. Bell, and J. B. Snider, 1994: The albedo of fractal stratocumulus clouds. *J. Atmos. Sci.,* **51,** 2434–2455.

Castleman, R. R., 1996: *Digital Image Processing.* Prentice Hall, 667 pp.

Clark, C., and J. Boyce, 1999: The detection of ship trail clouds by artificial neural network. *Int. J. Remote Sens.,* **20,** 711–726.

Comstock, K., C. S. Bretherton and S. E. Yuter, 2005: Mesoscale variability and drizzle in southeast Pacific stratocumulus. *J. Atmos. Sci.,* **62,** 3792–3807.

Considine, G., J. A. Curry, and B. Wielicki, 1997: Modeling cloud fraction and horizontal variability in marine boundary layer clouds. *J. Geophys. Res.,* **102,** 13 517–13 525.

Dai, A., and C. Deser, 1999: Diurnal and semidiurnal variations in global surface wind and divergence fields. *J. Geophys. Res.,* **104,** 31 109–31 125.

Davis, A., A. Marshak, W. Wiscombe, and R. Cahahlan, 1996: Scale invariance of liquid water distributions in marine stratocumulus. Part I: Spectral properties and stationarity issues. *J. Atmos. Sci.,* **53,** 1538–1558.

Han, Q., W. B. Rossow, and A. A. Lacis, 1994: Near global survey of effective droplet radii in liquid water clouds using ISCCP data. *J. Climate,* **7,** 465–497.

Jeffery, C. A., and P. H. Austin, 2003: Unified treatment of the thermodynamic and optical variability of unresolved low clouds. *J. Atmos. Sci.,* **60,** 1621–1631.

King, M. D., Y. Kaufman, W. P. Menzel, and D. Tanré, 1992: Remote sensing of cloud, aerosol, and water vapor properties from the moderate resolution imaging spectroradiometer (modis). *IEEE Trans. Geosci. Remote Sens.,* **30,** 2–27.

——, S.-C. Tsay, S. E. Platnick, M. Wang, and K.-N. Liou, 1997: Cloud retrieval algorithms for MODIS: Optical thickness, effective particle radius, and thermodynamic phase. MODIS Algorithm Theoretical Basis Doc. ATBD-MOD-05, NASA.

——, W. P. Menzel, and Y. Kaufman, 2003: Cloud and aerosol properties, precipitable water, and profiles of temperature and water vapor from modis. *IEEE Trans. Geosci. Remote Sens.,* **41,** 442–458.

Kistler, R., and Coauthors, 2001: The NCEP–NCAR 50-year reanalysis: Monthly means CD-ROM and documentation. *Bull. Amer. Meteor. Soc.,* **82,** 247–267.

Klein, S. A., 1997: Synoptic variability of low-cloud properties and meteorological parameters in the subtropical trade wind boundary layer. *J. Climate,* **10,** 2018–2039.

——, and D. L. Hartmann, 1993: The seasonal cycle of low stratiform clouds. *J. Climate,* **6,** 1588–1606.

Larson, V. E., R. Wood, P. R. Field, J.-C. Golaz, T. H. Vonder Haar, and W. R. Cotton, 2001a: Small-scale and mesoscale variability of scalars in cloudy boundary layers: One-dimensional probability density functions. *J. Atmos. Sci.,* **58,** 1978–1994.

——, ——, ——, ——, ——, and ——, 2001b: Systematic biases in the microphysics and thermodynamics of numerical models that ignore subgrid-scale variability. *J. Atmos. Sci.,* **58,** 1117–1128.

Ma, X., Z. Wan, C. Moeller, W. Menzel, L. Gumley, and Y. Zhang, 2000: Retrieval of geophysical parameters from moderate resolution imaging spectroradiometer thermal infrared data: Evaluation of a two-step physical algorithm. *Appl. Opt.,* **39,** 3537–3550.

Marshak, A., A. Davis, W. Wiscombe, and R. Cahalan, 1997: Scale invariance in liquid water distributions in marine stratocumulus. Part II: Multifractal properties and intermittency issues. *J. Atmos. Sci.,* **54,** 1423–1444.

Mellor, G. L., 1977: The Gaussian cloud model relations. *J. Atmos. Sci.,* **34,** 356–358.

Nicholls, S., and J. Leighton, 1986: An observational study of the structure of stratiform cloud sheets: Part i. Structure. *Quart. J. Roy. Meteor. Soc.,* **112,** 431–460.

Oreopoulos, L., and R. Davies, 1998a: Plane parallel albedo biases from satellite observations. Part I: Dependence on resolution and other factors. *J. Climate,* **11,** 919–932.

——, and ——, 1998b: Plane parallel albedo biases from satellite observations. Part II: Parameterizations for bias removal. *J. Climate,* **11,** 933–944.

Park, S., C. B. Leovy, and M. A. Rozendaal, 2004: A new heuristic Lagrangian marine boundary layer cloud model. *J. Atmos. Sci.,* **61,** 3002–3029.

Petters, M. D., J. R. Snider, B. Stevens, G. Vali, I. Faloona, and L. Russell, 2006: Accumulation mode aerosol, pockets of open cells, and particle nucleation in the remote subtropical Pacific marine boundary layer. *J. Geophys. Res.,* **111,** D02206, doi:10.1029/2004JD005694.

Pincus, R., and S. A. Klein, 2000: Unresolved spatial variability and microphysical process rates in large scale models. *J. Geophys. Res.,* **105,** 27 059–27 066.

——, M. Szczodrak, J. Gu, and P. Austin, 1995: Uncertainty in cloud optical depth estimates made from satellite radiance measurements. *J. Climate,* **8,** 1453–1462.

——, S. A. McFarlane, and S. A. Klein, 1999: Albedo bias and the horizontal variability of clouds in subtropical marine boundary layers: Observations from ships and satellites. *J. Geophys. Res.,* **104,** 6183–6191.

Reynolds, R. W., and T. M. Smith, 1994: Improved global sea surface temperature analyses using optimum interpolation. *J. Climate,* **7,** 929–948.

Rossow, W. B., and R. A. Schiffer, 1991: ISCCP cloud data products. *Bull. Amer. Meteor. Soc.,* **72,** 2–20.

——, C. Delo, and B. Cairns, 2002: Implications of the observed mesoscale variations of clouds for earth's radiation budget. *J. Climate,* **15,** 557–585.

Rotstayn, L. D., 2000: On the "tuning" of autoconversion parameterizations in climate models. *J. Geophys. Res.,* **105,** 15 495–15 507.

Schroder, M., R. Bennartz, L. Schuller, R. Preusker, P. Albert, and J. Fischer, 2002: Generating cloud masks in spatial high-resolution observations of clouds using texture and radiance information. *Int. J. Remote Sens.,* **23,** 4247–4261.

Shao, Q., and D. A. Randall, 1996: Closed mesoscale cellular convection driven by cloud-top radiative cooling. *J. Atmos. Sci.,* **53,** 2144–2165.

Sharon, T. M., B. A. Albrecht, H. Jonsson, P. Minnis, M. M. Khaiyer, T. M. VanReken, J. Seinfeld, and R. Flagan, 2006: Aerosol and cloud microphysical characteristics of rifts and gradients in maritime stratocumulus clouds. *J. Atmos. Sci.,* **63,** 983–997.

Slingo, J. M., 1980: A cloud parameterization scheme derived from GATE data for use with a numerical model. *Quart. J. Roy. Meteor. Soc.,* **106,** 747–770.

Smith, R. N. B., 1990: A scheme for predicting layer clouds and their water content in a general circulation model. *Quart. J. Roy. Meteor. Soc.,* **116,** 435–460.

Sommeria, G., and J. W. Deardorff, 1977: Subgrid-scale condensation in models of nonprecipitating clouds. *J. Atmos. Sci.,* **34,** 344–355.

Stevens, B., and Coauthors, 2005: Pockets of open cells (POCs) and drizzle in marine stratocumulus. *Bull. Amer. Meteor. Soc.,* **86,** 51–57.

Tompkins, A. M., 2002: A prognostic parameterization for the subgrid-scale variability of water vapor and clouds in large-scale models and its use to diagnose cloud cover. *J. Atmos. Sci.,* **59,** 1917–1942.

Wood, R., 2005: Drizzle in stratiform boundary layer clouds. Part I: Vertical and horizontal structure. *J. Atmos. Sci.,* **62,** 3011–3033.

——, and P. R. Field, 2000: Relationships between total water, condensed water, and cloud fraction in stratiform clouds examined using aircraft data. *J. Atmos. Sci.,* **57,** 1888–1905.

——, and J. P. Taylor, 2001: Liquid water path variability in unbroken marine stratocumulus. *Quart. J. Roy. Meteor. Soc.,* **127,** 2635–2662.

——, and C. S. Bretherton, 2004: Boundary layer depth, entrainment and decoupling in the cloud-capped subtropical and tropical marine boundary layer. *J. Climate,* **17,** 3576–3588.

——, P. R. Field, and W. R. Cotton, 2002: Autoconversion rate bias in boundary layer cloud parameterizations. *Atmos. Res.,* **65,** 109–128.

Wyant, M. C., C. S. Bretherton, J. T. Bacmeister, J. T. Kiehl, I. M. Held, Z. M. S. A. Klein, and B. A. Soden, 2006: A comparison of tropical cloud properties and responses in gems using mid-tropospheric vertical velocity. *Climate Dyn.,* in press.